Dalton Transactions

Accepted Manuscript

ROYAL SOCIETY OF CHEMISTRY

www.rsc.org/dalton

Journal Name

ARTICLE

Covalent Bridging of Surface Functionalized Fe_3O_4 and YPO_4: Eu Nanostructures for Simultaneous Imaging and Therapy

Received 00th January 20xx,
Accepted 00th January 20xx

DOI: 10.1039/x0xx00000x

www.rsc.org/

K. C. Barick[a,*], Anusha Sharma[a], Neena G. Shetake[b], R. S. Ningthoujam[a], R. K. Vatsa[a], P. D. Babu[c], B. N. Pandey[b] and P. A. Hassan[a,*]

Magnetic luminescent hybrid nanostructures (MLHN) have received a great deal of attention due to their potential biomedical applications such as thermal therapy, magnetic resonance imaging, drug delivery and intracellular imaging. We report the development of bifunctional Fe_3O_4 decorated YPO_4: Eu hybrid nanostructures by covalent bridging of carboxyl PEGylated Fe_3O_4 and amine functionalized YPO_4: Eu particles. The surface functionalization of individual nanoparticulates as well as their successful conjugation was evident from Fourier transform infrared spectroscopy (FTIR), dynamic light scattering (DLS), zeta-potential and transmission electron microscopy (TEM) studies. X-ray diffraction (XRD) analysis reveals the formation of highly crystalline hybrid nanostructures. TEM micrographs clearly show the binding/ anchoring of 10 nm Fe_3O_4 nanoparticles onto the surface of 100-150 nm rice grain shaped YPO_4: Eu nanostructures. These MLHN show good colloidal stability, magnetic field responsivity and self-heating capacity under external AC magnetic field. The induction heating studies confirmed localized heating of MLHN under AC magnetic field with high specific absorption rate. Photoluminescence spectroscopy and fluorescence microscopy results show optical imaging capability of MLHN. Furthermore, successful internalization of these MLHN in the cells and their cellular imaging ability are confirmed from confocal microscopy imaging. Specifically, the amine functionalized YPO_4: Eu nanostructure provides an excellent platform to integrate luminescent and magnetic materials into one single entity that can be used as a potential tool for hyperthermia treatment of cancer and cellular imaging.

Introduction

Recently, hybrid nanomaterials have received a great deal of attention due to their potential applications in catalysis, biological sensing and biomedical imaging etc.[1-3] The hybrid structure composed of magnetic and luminescent inorganic nanoparticles are of particular importance because they offer a number of novel applications in biotechnology and nanomedicine. It is also expected that integrating magnetic and luminescent properties into a single entity, would enable the engineering of unique nanoscale devices which can exhibit multiple functions and could be manipulated using external magnetic field.[4] Fe_3O_4 magnetic nanoparticles (MNPs) have attracted much attention because of their unique physio-chemical properties and potential biomedical applications such as magnetic hyperthermia, targeted drug delivery, magnetic resonance imaging and separation science.[5-9] Among these applications, the hyperthermia capability of Fe_3O_4 nanoparticles has drawn remarkable interest due to its ability for heat activated killing of cancerous cells at 5-7 ^{o}C above the body temperature.[10,11] This is due to the fact that cancer cells are more sensitive to heat damage as compared to healthy cells.[12] One of the attractive features of MNPs is that they can be relatively easily functionalized with different molecules which may provide new properties on the particles. Combination cellular imaging with hyperthermia permits verification and quantification of treatment, and can serve as an efficient modality for site specific therapy for cancer. Further, the MNPs coated with specific fluorescent probe can provide detailed understanding of cellular processes at the molecular level. With this objective, fluorescent organic dye molecules and quantum dots (QDs) tagged multifunctional magnetic particles have been developed by various groups and their ability to overcome the limitations of conventional therapy has been demonastrated.[13-15] However, both fluorescent organic dye molecules and QDs, suffer from inherent limitations especially quenching and toxicity, which thereby limits their application in therapeutic and in-vivo studies.

Recently, less toxic rare-earth based luminescent nanomaterials have emerged as a new class of biological labeling agents. They offer various advantages over organic fluorescent molecules and QDs such as high photochemical stability, long luminescence lifetime and high quantum yield.[16-18] For instance, Di et al. have synthesized luminescent Eu doped $TbPO_4$ nanoparticles and reported their *in-vitro* imaging capability.[18] Report on rare-earth based luminescent nanomaterials integrated with MNPs are rather scarce. Wang et al. reported fabrication of Fe_3O_4@YPO_4: Ln (Ln = Tb, Eu) multifunctional magnetic-fluorescent hybrid spheres and investigated their imaging capability.[19] Recently, Prasad and co-workers have investigated the hyperthermia application of Fe_3O_4@YPO_4:Eu hybrid nanoparticles. They have prepared these hybrid nanoparticles by direct precipitation of YPO_4: Eu over Fe_3O_4.[20] However, it is important to engineer the surface of nanoparticles with desired functionality that can provide colloidal stability, biocompatibility and site for conjugation of drugs/ biomolecules.

Herein, we report the design and development of amine functionalized YPO_4: Eu and carboxyl functionalized Fe_3O_4 nanoparticles, which were then covalently conjugated to create a

[a]*Chemistry Division, Bhabha Atomic Research Centre, Mumbai – 400085, India. E-mail: kcbarick@barc.gov.in (K. C. Barick), hassan@barc.gov.in (P. A. Hassan), Fax: + 91 22 2550 5151, Tel: + 91 22 2559 0284.*
[b]*Radiation Biology and Health Sciences Division, Bhabha Atomic Research Centre, Mumbai – 400085, India.*
[c]*UGC-DAE Consortium for Scientific Research, Mumbai – 400 085, India.*

† Electronic Supplementary Information (ESI) available: Cell culture procedure, photograph of induction coil, TEM images, normalized absorbance vs. time plot, magnetization plots, emission and excitation spectra, fluorescence image and protein-particle interaction (Fig. S1-S8, Table S1). See DOI: 10.1039/x0xx00000x.

single entity exhibiting both magnetic and luminescent properties. The good aqueous colloidal stability, low toxicity and excellent self-heating efficacy make these novel magnetic luminescent hybrid nanostructures (MLHN) suitable for hyperthermia treatment of cancer. The luminescent entity helps us to identify the location of MNPs during in-vitro cellular imaging.

Experimental

Materials

Ferrous chloride tetrahydrate ($FeCl_2.4H_2O$), ferric chloride hexahydrate ($FeCl_3.6H_2O$), PEG-diacid (poly (ethylene glycol) bis (carboxymethyl) ether, M_n = 600), yttrium oxide (Y_2O_3), europium nitrate hexahydrate ($Eu(NO_3)_3.6H_2O$), tetraethoxysilane (TEOS), *N*-hydroxysuccinimide (NHS), 3-aminopropyltrimethoxysilane (APTES), 3-(4,5-dimethyl-2-thiazolyl)-2,5-diphenyl-2H-tetrazolium bromide (MTT) and bovine serum albumin (BSA) were purchased from Sigma-Aldrich, USA. Dulbecco's modified Eagle medium (DMEM) and fetal calf serum (FCS) were obtained from Invitrogen, USA and Himedia Laboratories, India, respectively. Ammonia solution was procured from Thomas Baker Chemical Pvt. Ltd., India. 1-Ethyl-3-(3-dimethylaminopropyl*)* carbodiimide hydrochloride (EDC. HCl) was obtained from SRL, India. Ethylene glycol (EG) and polyethylene glycol (PEG) were purchased from Spectrochem, India. Concentrated nitric acid (HNO_3) and dimethyl sulfoxide (DMSO) were obtained from SD Fine Chemicals and E. Merck Ltd., India, respectively. Absolute ethanol was procured from Changshu Yangyuan Chemical, China. All chemicals are of analytical grade and used without further purification.

Preparation of amine functionalized YPO_4: Eu luminescent nanoparticles (AFLN)

For the preparation of 10 at. % Eu^{3+} doped YPO_4 (YPO_4: Eu), 0.5 g (2.2×10^{-3} mol) of Y_2O_3 was dissolved in 2 ml of conc. HNO_3 in a round bottom flask and then it was heated at ~80 ^oC to get a clear solution. 0.207 g (4.64×10^{-4} mol) of $Eu(NO_3)_3.6H_2O$ was added to the above solution and the solution was further heated at ~80-100 ^oC to remove excess of HNO_3 acid, by alternate addition of 2-3 ml of milli Q water. The evaporation process was repeated 4-5 times. To this 30 ml of EG and 10 ml of PEG were added, followed by addition of 10 ml aqueous solution of $(NH_4)H_2PO_4$ (1.08 g, 9.38×10^{-3} mol). The reaction mixture was heated at 140-160 ^oC for 2 h. The white precipitate that appeared was separated by centrifugation (8000 rpm, 10 min), washed 3-4 times with Milli Q water and dried under ambient conditions.

Amine functionality was introduced through a modified Stöber method.[21] In a typical experiment, 60 mg of YPO_4: Eu particles were dispersed in 210 ml ethanol and sonicated at room temperature for 1 h. Then a solution of 15 ml of 15% $NH_3.H_2O$ was added to the above mixture and sonicated for 15 min. This is followed by drop wise simultaneous addition of 60 µl of TEOS and 600 µl of APTES. The reaction mixture was stirred for 1 h at room temperature. Subsequently, the resulting amine functionalized luminescent nanoparticles (AFLN) were washed with Milli Q water followed by centrifugation (8000 rpm, 10 min) and ultrasonication. These samples were dried at 60 °C prior to further studies.

Preparation of carboxyl functionalized Fe_3O_4 magnetic nanoparticles (CFMN)

The carboxyl functionalized Fe_3O_4 magnetic nanoparticles (CFMN) were synthesized through co-precipitation of Fe^{2+} and Fe^{3+} in basic medium followed by *in-situ* coating of PEG-diacid as reported elsewhere.[22] In a typical synthesis, 1.988 g (0.01 mol) of $FeCl_2.4H_2O$ and 5.406 g (0.02 mol) of $FeCl_3.6H_2O$ were dissolved in 80 ml of water in a round bottom flask and temperature was slowly increased to 70 ^oC under N_2 atmosphere with constant mechanical stirring at 1000 rpm. The temperature was maintained at 70 ^oC for 30 min and then 30 ml of 25% ammonia solution was added instantaneously to the reaction mixture, and kept for another 30 min at 70 ^oC. Then, 5 ml PEG-diacid was added and temperature was slowly raised up to 90 ^oC and reacted for 60 min with continuous stirring. The obtained black colored CFMN were then thoroughly rinsed with water and separated from the supernatant using a permanent magnet (~2.5 kOe).

Preparation of magnetic-luminescent Fe_3O_4-YPO_4: Eu hybrid nanostructures (MLHN)

Magnetic-luminescent Fe_3O_4-YPO_4: Eu hybrid nanostructures (MLHN) were prepared by EDC-NHS coupling between 4:1 weight ratios of AFLN and CFMN. Typically, 7.5 mg of CFMN were dispersed in 100 ml of milli Q water for 30 min through sonication to get a homogeneous solution. 0.5 ml EDC. HCl (2 mg/ml, 10.43 mM) is added to the above solution and sonicated for another 20 min, after which 1 ml NHS (1 mg/ml, 8.68 mM) was added with further sonication for 20 min. 30 mg AFLN were dispersed in 50 ml milli Q water through sonication for 30 min and added to the solution of EDC-NHS activated CFMN. This reaction mixture was kept under mechanical stirring for 3 h. The obtained MLHN were then separated from the supernatant using a permanent magnet and thoroughly rinsed with water. The schematic representation for the preparation of MLHN by EDC-NHS coupling reaction is shown in scheme 1.

Characterizations

The crystal structure of the material was identified by Phillips PW1729 diffractometer with CuKα radiation. The average crystallite size is estimated from the X-ray line broadening (three most intense peaks) using Scherrer formula:

$$D = \frac{0.89\,\lambda}{\beta \cos\theta}$$

where, D is crystallite size, λ is wavelength of Cu Kα and β is full width at half maximum of the diffraction peak. Infrared spectra were recorded in the range 4000-400 cm^{-1} on a Fourier transform infrared spectrometer (FTIR, Bomem, MB series). The transmission electron micrographs were taken by Philips 200 TEM for particle

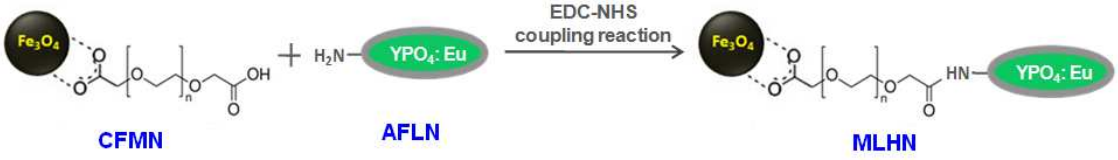

Scheme 1. Schematic representation of the preparation of MLHN by EDC-NHS coupling.

size determination. Dynamic light scattering (DLS) measurement was performed using a Malvern 4800 Autosizer employing a 7132 digital correlator for the determination of hydrodynamic diameter. The zeta-potential measurements were performed by Zetasizer nano series, Malvern Instruments. Colloidal stability assay was investigated by measuring the absorbance of MLHN suspensions (0.5 mg/ml) in different mediums at a wavelength of 350 nm using JASCO V-650, UV-visible spectrophotometer. The field-dependence magnetization (M vs. H) of MLHN at 5 and 300 K, and their temperature-dependent magnetization under zero-field cooled (ZFC) and field-cooled (FC) conditions in an applied field of 100 Oe were measured by physical properties measurement system (PPMS), Quantum Design. The room temperature photoluminescence (PL) spectra of these powder hybrid nanostructures were recorded using Edinburgh Instrument FLS920 having 450 W Xe lamp as a source (μW power). Fluorescence microscopy image has been collected using Olympus BX 100 microscope. The estimation of carboxyl and amine groups present on surface of samples were carried out by using standard protocols of methylene blue adsorption and ninhydrin method, respectively.

The heating ability of the FLNH and MLHN suspensions has been obtained from the time-dependent calorimetric measurements using an induction heating unit (East Heat 8310, Ambrell). 1 ml aqueous suspensions (1 mg/ml of Fe) of samples were taken in an eppendorf tube with suitable arrangements (eppendorf tube was kept at the centre of induction coil with the support of thermocol, Fig. S1, ESI†) to minimize the heat loss. The specific absorption rate (SAR) values were determined at different AC magnetic fields with a fixed frequency of 265 kHz. The SAR was calculated using the following equation:

$$SAR = C\frac{\Delta T}{\Delta t}\frac{1}{m_{Fe_3O_4}}$$

where, C is the specific heat of solvent ($C = C_{water} = 4.18$ J/g °C), $\Delta T/\Delta t$ is the initial slope of the time-dependent temperature curve and $m_{Fe_3O_4}$ is mass fraction of Fe_3O_4 in the sample.

The heat activated killing of cancer cells (A549, human lung carcinoma) was evaluated under AMF using appropriate controls by MTT assay. Cells (0.25×10^6) were seeded overnight in petridishes (P-30) containing 2 ml culture medium (complete DMEM) followed by treatment with MLHN (4 mg) for 3 h under culture conditions. Then, cultures were subjected to AMF (0.335 kOe) for 10 min under sterile conditions using an induction heating unit. After AMF exposure, cells were further cultured for 48 h. Then, the media containing nanoparticles was carefully removed and processed for the MTT assay to determine the cell viability (details of cell culture procedure are provided in ESI†). Cells treated with different conditions are referred to as follows: (i) control cells (C), (ii) cells with AMF only (H), (iii) MLHN particles only (P) and (iv) cells treated with particles followed by exposure of AMF (P + H).

Intracellular luminescence imaging of hybrid nanostructure was carried out by confocal laser scanning microscopy (CLSM) using A549 cell line. For confocal microscopy imaging, cells (0.5×10^6) were seeded on glass coverslips and cultured overnight. The cells were then treated with 1 mg/ml of MLHN for 3 h in culture conditions, followed by washing with PBS. Later, the cells were treated with lysotracker green for 10 min at culture conditions, followed by washing with PBS. The cells were then mounted on a slide using Prolong Gold antifade (Molecular probes, USA) containing DAPI, for nuclear staining, followed by imaging using CLSM (LS510 Meta, Carl Ziess). The excitation source used was an Ar ion laser with a power of mW (364 nm for DAPI and MLHN, and 488 nm for lysotracker green) and the emission window was set at 385–470 nm, 505-520 and 575-615 nm for DAPI, lysotracker green and MLHN, respectively.

Results and discussion

The YPO_4: Eu and Fe_3O_4 are chosen as luminescent and magnetic materials for preparation of hybrid nanostructure due to their strong luminescent and magnetic properties, respectively. We have introduced a thin silica shell (8-10 nm) having amine functionality (SiO_2-NH_2) to YPO_4: Eu nanostructure as its surface is incompatible for direct linking with Fe_3O_4 MNPs. The thin SiO_2-NH_2 shell not only provides amine functionality for the conjugation of carboxyl functionalized Fe_3O_4 MNPs but also act as effective barrier to quenching of the luminescence property of YPO_4: Eu.

Fig. 1 shows XRD patterns of AFLN, CFMN and MLHN (inset shows the expanded encircled region of the XRD pattern of MLHN). The XRD pattern of AFLN shows the presence of two phases of YPO_4: Eu, i.e. tetragonal (JCPDS card no. 11-0254) and hexagonal phase (JCPDS card no. 42-0082). The XRD pattern of CFMN reveals the formation of single-phase Fe_3O_4 inverse spinel structure (JCPDS Card No. 88-0315 for magnetite). The presence of sharp peaks in both AFLN and CFMN confirmed formation of respective highly crystalline nanoparticles. The crystallite sizes of AFMN and CFMN are estimated about 44 and 10 nm, respectively from X-ray line broadening using Scherrer formula. The appearance of diffraction peaks of both Fe_3O_4 and YPO_4: Eu in MLHN suggested the formation of hybrid nanostructures (confirmed from FTIR and TEM results shown later). Furthermore, the diffraction peaks from YPO_4: Eu are more dominant than those from Fe_3O_4, because the hybrid nanostructures are made of smaller Fe_3O_4 nanoparticles assembled around larger individual YPO_4: Eu and have a higher percentage of YPO_4: Eu.

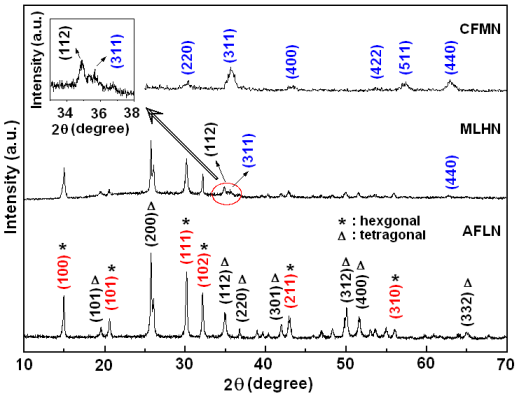

Fig. 1. XRD patterns of AFLN, CFMN and MLHN (inset shows the expanded encircled region of XRD pattern of MLHN).

The surface chemical structure is characterized by FTIR spectroscopy. Fig. 2 shows the FTIR spectra of (a) CFMN (b) AFLN and (c) MLHN. From FTIR spectrum of CFMN (Fig. 2a), it can be observed that the characteristic C=O band of PEG-diacid at 1742 cm^{-1} is significantly reduced and an additional intense band appeared at a lower wavenumber (1635 cm^{-1}, COO^- asymmetric stretching). This spectral change indicates binding of some of the carboxylate group of PEG-diacid with Fe_3O_4.[23] However, the presence weak C=O vibration at 1742 cm^{-1} in CFMN suggests the

presence of some free carboxyl groups on the surface of Fe_3O_4 nanoparticles. Earlier investigations also suggested that one carboxylate head is the preferable site for chemical conjugation with Fe_3O_4 leaving the other one free.[24,25] Further, the vibrational modes appeared at 1460 cm^{-1} (COO^- symmetric stretching), 1025 cm^{-1} (carboxylic -OH bend), and 3420 cm^{-1} (carboxylic -OH stretching) in CPMN indicates the presence of PEG-diacid on the Fe_3O_4 nanoparticles. The strong IR band observed at around 580 cm^{-1} in CFMN can be ascribed to the Fe-O stretching vibrational mode of Fe_3O_4.[8]

In FTIR spectrum of AFLN (Fig. 2b), the bands appeared at around 530 and 630 cm^{-1} correspond to bending vibrations of PO_4^{3-} and the intense broad band in the range of 900-1300 cm^{-1} can be attributed to stretching vibrations of PO_4^{3-}.[26] The bands at 3455 and 1620 cm^{-1} can be ascribed to the N–H stretching vibration and NH_2 bending mode of free NH_2 groups.[27] This indicates that the coupling agent APTES has been introduced onto the surface of luminescent YPO_4: Eu particles. In FTIR spectrum of MLHN (Fig. 2c), two additional vibrational modes appeared at 1540 cm^{-1} and 1655 cm^{-1} corresponding to the vibrations of N-H (amide II band) and C=O (amide I band), respectively along with characteristic vibrations of Fe-O and PO_4^{3-}.[6,28] These additional vibrations in hybrid nanostructure suggest the formation of amide linkage between CFMN and AFLN.

From TEM micrograph of CFMN (Fig. 3a), it is evident that Fe_3O_4 nanoparticles are nearly spherical in shape with an average crystallite size of ~ 10 nm, which is comparable to the results obtained from XRD. TEM micrographs of AFLN (Fig. 3b and Fig. S2a, ESI†) depict the formation of rice grain shaped YPO_4: Eu particles having width of ~ 50 nm and length of 100-150 nm. The uniform coating silica on the surface of YPO_4: Eu particles are clearly observed from TEM images. The average interplanar distance of AFLN was measured to be 0.34 nm (Fig. 3c), which was assigned to the (200) plane of YPO_4: Eu. In case of hybrid nanostructures (Fig. 3d and Fig S2b, ESI†), it has been observed that Fe_3O_4 nanoparticles are randomly decorated onto the surface of aminosilane coated YPO_4: Eu particles. The smooth surface of aminosilane coated YPO_4: Eu became rough after conjugation of Fe_3O_4 nanoparticles. Furthermore, the individual features of CFMN and AFLN can be seen in electron diffraction pattern of hybrid structures (Fig. 3e-g).

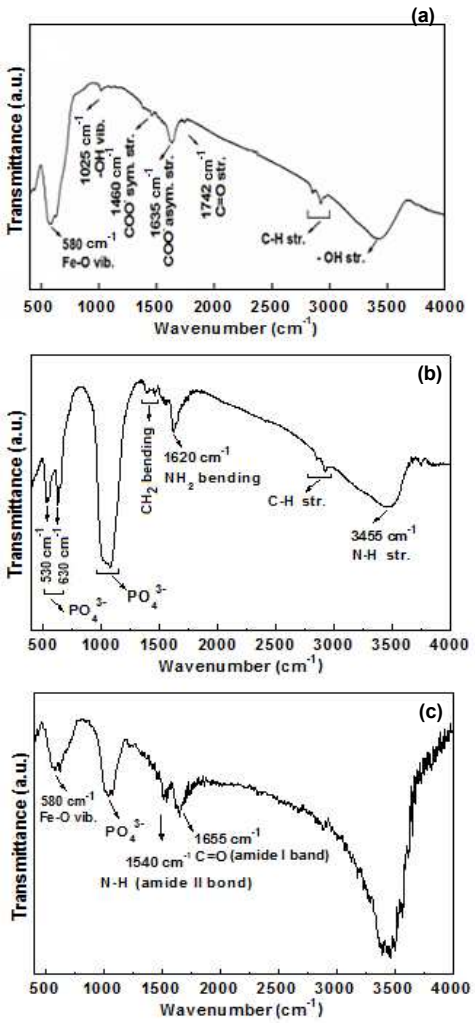

Fig. 2. FTIR spectra of (a) CFMN, (b) AFLN and (c) MLHN.

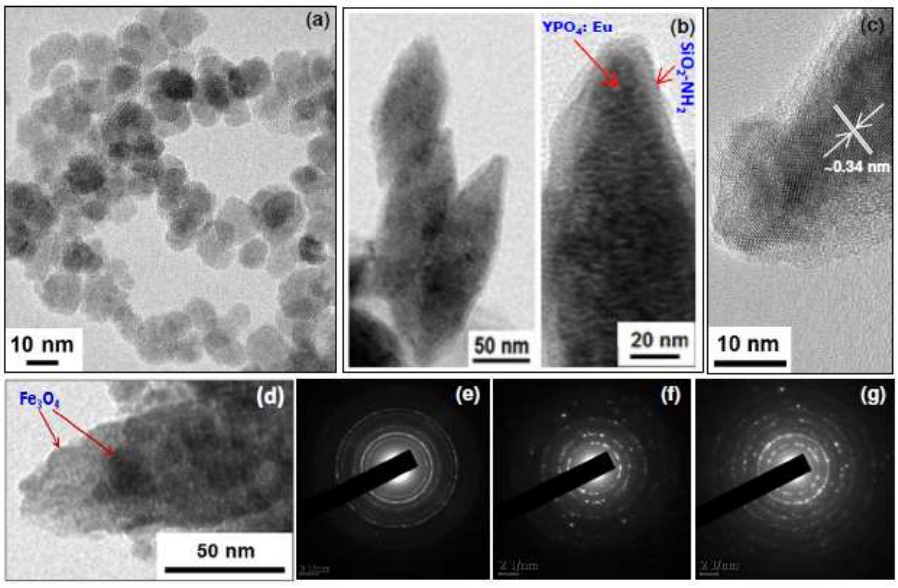

Fig. 3. (a) TEM micrographs of CFMN, (b) TEM micrographs of AFLN, (c) HRTEM micrograph of AFLN, (d) TEM micrograph of MLHN, and SAED patterns of (e) CFMN, (f) AFLN and (g) MLHN.

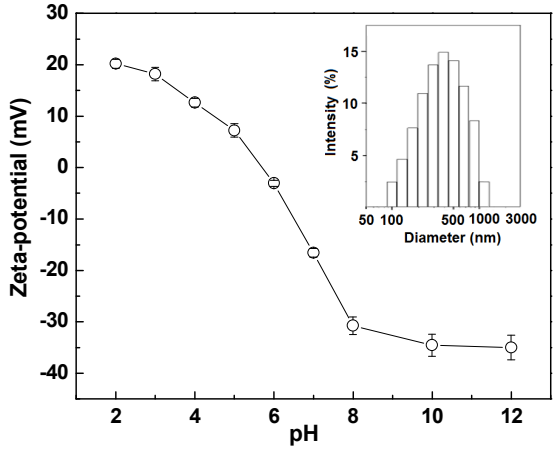

Fig. 4. Variations in zeta-potential of aqueous suspension of MLHN at different pH values. Inset shows the DLS plot of MLHN at pH 7.

Colloidal stability in aqueous and physiological medium is one of the most important issues relating to the biomedical applications of the nanohybrid system. The pH dependent charge conversional behaviour was monitored using zeta-potential measurements of the hybrid system. Fig. 4 shows the variation in zeta-potential of aqueous suspension of MLHN at different pH. At neutral pH, the MLHN have surface charge of -16.5 mV which further increases with increase in basicity due to the presence of ionized carboxyl groups. At low pH (pH ≤ 4), the surface potential becomes positive due to protonation of the free NH_2 groups present on the surface of the hybrid system. Further, DLS measurement (inset of Fig. 4) indicates that the prepared particles exist as a colloidal suspension with mean intensity average (z-average) hydrodynamic diameter of about 300 nm (polydispersity index = 0.25) due to the presence of associated and hydrated organic layers.[8,29] The increase in size obtained from DLS, as compared to TEM could also arise from the z-average diameter (as opposed to number average in TEM) of a polydisperse population of particles.

The dispersibility and colloidal stability of the particles were also assessed from the changes in light scattering intensity as well as extinction changes with time. The dispersibility is evident from the increase in absorbance and scattering intensity of the sample when dispersed in aqueous and cell culture media (DMEM + 10% FBS). The insignificant change in absorbance of MLHN suspensions in aqueous and culture media indicates their good colloidal stability (Fig. S3, ESI†). As described earlier, the Fe_3O_4 decorated YPO_4: Eu nanohybrid was achieved through the covalent coupling between carboxyl and amine groups by EDC-NHS reaction. Here, Fe_3O_4 and YPO_4: Eu were separately functionalized with carboxyl-terminated PEG and amine-terminated silane, respectively and then reacted at room temperature for further conjugation. The amount of carboxyl and amine groups present on surface of CFMN and AFLN were found to be 1.2 and 1.5 mmol/g, respectively. However, hybrid nanostructures formed by conjugation of CFMN and AFLN have 0.52 mmol/g of carboxyl groups. This indicates that the MLHN still possess free carboxyl and amine groups on their surface. We believe that these free amine and carboxyl groups make the hybrid nanostructures hydrophilic by formation of hydrogen bonds between surface functional groups and water. In addition, the electrostatic repulsive force originating from the ionization/ protonation of the surface groups provide additional stability to the particles.

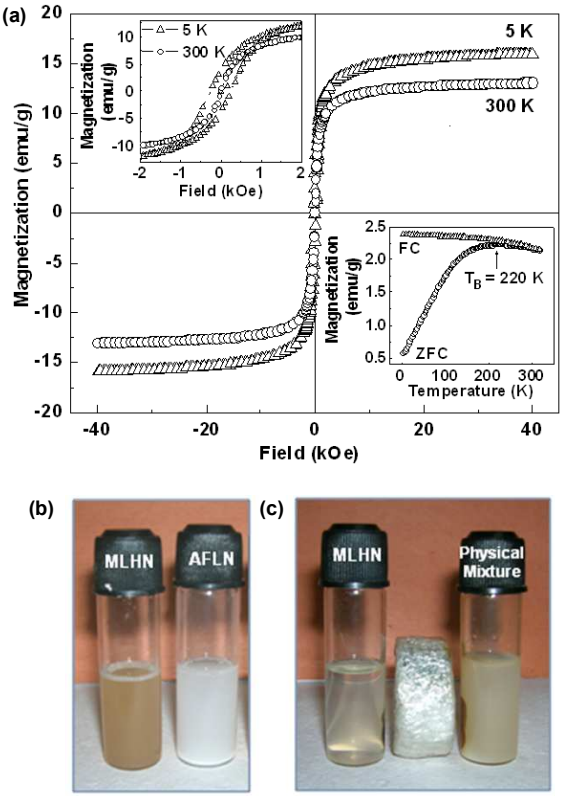

Fig. 5. (a) Field dependent magnetization (M vs. H) plots of MLHN at 5 and 300 K (top inset: expanded M vs. H plot of MLHN at low field region, bottom inset: temperature dependence of the magnetization plots of MLHN), (b) aqueous colloidal suspensions of MLHN and AFMN, and (c) suspension of MLHN and physical mixture of AFMN and CFMN in presence of external magnet of field strength ~ 2.5 kOe.

In order to assess the ability of MLHN in hyperthermia applications, we investigated their magnetic field responsivity and heating efficacy. Fig. 5 shows (a) field dependent magnetization (M vs. H) plots of MLHN at 5 and 300 K (top inset: expanded M vs. H plot of MLHN at low field region, bottom inset: temperature dependence of the magnetization plots of MLHN), (b) aqueous colloidal suspensions of MLHN and AFMN, and (c) aqueous suspension of MLHN and physical mixture of AFMN and CFMN in presence of external magnet (field strength ~ 2.5 kOe). At 300 K, samples exhibit superparamagnetic behaviour without magnetic hysteresis and remanence, whereas ferromagnetic behaviour with a coercivity of 250 Oe is observed at 5 K (Fig. 5a and its top inset). This transition from superparamagnetic behaviour at high temperature to ferromagnetic behaviour below the so-called blocking temperature (T_B) is typically observed in magnetic nanoparticles.[30] The ZFC-FC plot (bottom inset of Fig. 5a) shows that the T_B of the MLHN is 220 K, as one would expect for superparamagnetic nanoparticles. The maximum magnetizations of MLHN (at an applied field of 40 kOe) were found to be 16 and 13 emu/g of sample at 5 and 300 K, respectively. The low value of magnetization can be attributed to the presence of large amount of non-magnetic luminescent component. It has been observed that MLHN are highly dispersible in water, but they are attracted

towards the permanent magnet in presence of its magnetic field. However, only CFMN (magnetic) were attracted towards the magnet leaving the AFLN (non-magnetic) in aqueous solution from physical mixture of magnetic and luminescent particles. These results further confirmed the successful formation of hybrid nanostructures of magnetic and luminescent particles through EDC-NHS coupling. From magnetic measurements, it may be noted that the retention of superparamagnetic property at room temperature with good magnetic field responsivity makes these nanostructures suitable for drug delivery and hyperthermia applications.

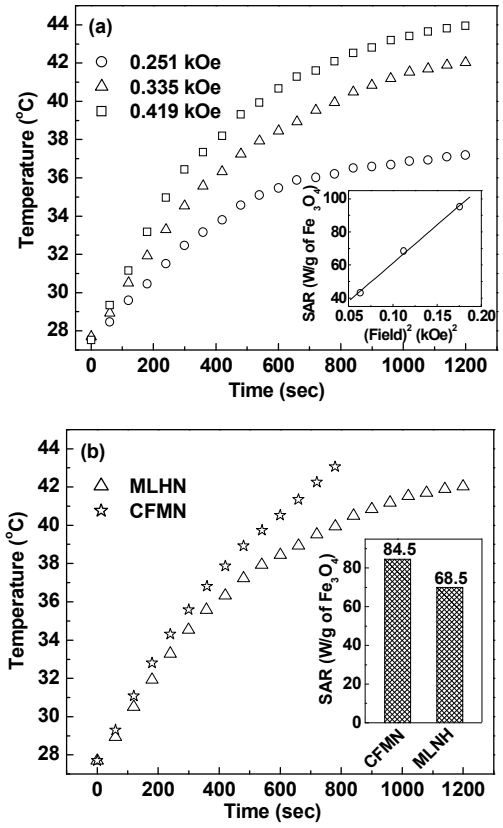

Fig. 6. Temperature vs. time plots of (a) MLHN at different AC magnetic field (inset: plot showing linear relationship between SAR and $(Field)^2$), and (b) CFMN and MLHN at AC magnetic field of 0.335 kOe (inset: plot showing their SAR values).

The temperature *vs.* time plots of MLHN suspensions showed a time-dependent gradual increase in temperature under AC magnetic fields (Fig. 6a). It has been observed that a magnetic field of 0.335 and 0.419 kOe at fixed frequency of 265 kHz is able to produce energy enough for raising the temperature of the magnetic suspension of 1 mg/ml of Fe to 42-43 ^{o}C (hyperthermia temperature) within 20 min. Further, the time required to reach hyperthermia temperature decreases with an increase in field strength, which is obvious as the heat generation/dissipation (*P*) is proportional to the square of applied AC magnetic field (inset of Fig. 6a) as follows[31,32]:

$$P = \pi\mu_0\chi_0 H^2 f \frac{2\pi f\tau_{eff}}{1+(2\pi f\tau_{eff})^2}$$

where, μ_0 is the permeability of free space, χ_0 is the magnetic susceptibility, *H* is the magnetic field amplitude and τ_{eff} is the effective relaxation time.

In thermal activation of Fe_3O_4 nanoparticles under AC magnetic field, an increase in temperature is mainly due to the combined effect of Néel and Brownian relaxations. The Néel and Brownian relaxation losses are associated with the magnetic moment rotations within the particles (due to internal fluctuations of the magnetic moment with respect to the crystal lattice) and with the entire particles (due to mechanical friction with the surrounding medium when nanoparticles keep oscillating toward the field, keeping its magnetic moment fixed along the crystal axis), respectively. The relaxation times are given by the following equations[31,32]:

$$\tau_N = \tau_0 e^{KV_M/k_BT}$$

$$\tau_B = \frac{4\pi\eta R_H^{\,3}}{k_BT}$$

$$\tau_{eff} = \frac{\tau_N\tau_B}{\tau_N+\tau_B}$$

where, τ_B is the Brownian relaxation time, τ_N is the Néel relaxation time, $\tau_0 \approx 10^{-9}$ s, *K* is the anisotropy constant, V_M is the volume of the Fe_3O_4 nanoparticle, k_B is Boltzmann's constant, *T* is temperature, η is the viscosity and R_H is the hydrodynamic particle radius. The use of magnetic nanoparticles in hyperthermia therapy depends on their heating efficiency, which is expressed in terms of the specific absorption rate (SAR). The SAR values of MLHN were found to be 43.3, 68.5 and 95.3, W/g of Fe_3O_4 with an applied field of 0.251, 0.335 and 0.419 kOe, respectively (at a fixed frequency of 265 kHz). The observed good SAR is likely to be due to a combination of their good magnetic responsivity (Néel relaxation time is sensitive to the magnetic field strength of particles) and aqueous colloidal stability (Brownian relaxation time is sensitive to colloidal stability of particles). Further, we have compared the heating efficacy of MLHN with CFMN at an applied AC magnetic field of 0.335 kOe and observed that the rate of heating is slower for MLHN (Fig. 6b). The SAR value of CFMN at 0.335 kOe was found to be 84.5 W/g of Fe_3O_4 with an applied field of 0.251 kOe, which is higher than that of MLHN (inset of Fig. 6b). The decrease in SAR for MLHN is mainly due to the presence of large amount of non-magnetic component in the sample. Furthermore, SAR is also dependent on other parameters such as amount of particles in suspension, magnitude of frequency and physical properties of MNPs (magnetization, particles size, size distribution and hydrodynamic radius of particles).[33] Therefore, the observed SAR values should not be viewed in terms of performances, but only as a demonstration that these magnetic hybrid nanostructures are excellent heating source for hyperthermia treatment of cancer.

Fig. 7 shows excitation spectra of AFLN and MLHN by monitoring emission (λ_{em}) at a wavelength of 612 nm, and their emission spectra recorded at excitation (λ_{ex}) wavelengths of (b) 260 and (c) 395 nm using 375 and 455 nm filters, respectively. The excitation spectrum of AFLN shows a broad (in the range of 230-280 nm) band centred at 260 nm corresponding to the Eu–O charge transfer band (CTB).[34,35] The appearance of intense Eu–O charge transfer band suggests strong energy transfer from Eu–O to Eu^{3+}. However, there is a shift of the centre of Eu-O CTB from 260 to 255 nm for MLHN. The change in position of CTB depends on the particle size of host

and environment of Eu^{3+}. The general f-f transitions (marked in Fig. 7a) can also be observed at 318, 361, 380 and 395 nm, respectively.[36,37] However, the overall intensity of these bands in MLHN slightly reduced as compared to those of AFLN possibly due to presence of magnetic component.

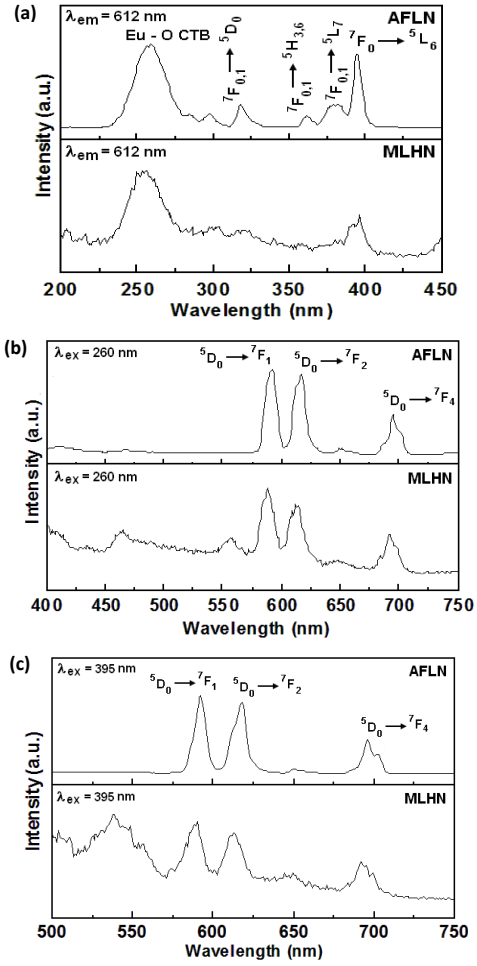

Fig. 7. (a) Excitation spectra of AFLN and MLHN by monitoring wave length at 612 nm, and their emission spectra recorded at excitation wavelengths of (b) 260 and (c) 395 nm using 375 and 455 nm filters, respectively.

The emission spectra taken at excitation wavelengths of 260 and 395 nm (Fig. 7b and 7c) exhibit typical emission peaks of Eu^{3+} corresponding to magnetic dipole transition, MDT ($^5D_0 \rightarrow {}^7F_1$) and electric dipole transitions, EDT ($^5D_0 \rightarrow {}^7F_2$ and $^5D_0 \rightarrow {}^7F_4$).[34,38] Among these emissions peaks, the intensity of the $^5D_0$–$^7F_2$ transition is predominant, hence the product shows red emission (discussed later). The wavelengths corresponding to magnetic and electric dipole transition of Eu^{3+} in AFLN and MLHN are shown in Table 1. In case of MLHN, a slight blue shift of emission peaks was observed as compared to AFLN luminescent particles. Further, the emission intensity is more when samples are excited at wavelength of 260 nm (Eu-O CTB) than 395 nm. This suggests strong energy transfer from Eu-O to Eu^{3+}. Apart from these, a weak peak centred at ~ 650 nm can also be observed in the emission spectra.

The asymmetric environment of Eu^{3+} in host lattice can be calculated by intensity ratio of the electric ($^5D_0 \rightarrow {}^7F_2$) to magnetic ($^5D_0 \rightarrow {}^7F_1$) dipole transitions. This is called as asymmetric ratio (A_{21}) and defined as:

$$A_{21} = \frac{\int_{603}^{636} I_2 \, d\lambda}{\int_{570}^{603} I_1 d\lambda}$$

where, I_1 and I_2 are the intensity of electric and magnetic dipole transitions, respectively. The A_{21} values for samples excited at the wavelengths of 260 and 395 nm are also included in Table 1. All calculations were carried from the integrated area under curve after removal of background. The insignificant change in A_{21} for hybrid nanostructures clearly suggests that the existence of Fe_3O_4 does not influence Eu^{3+} environment in YPO_4: Eu. It is noteworthy to mention that both magnetic and luminescent properties of hybrid nanostructures can be tuned by varying the weight percentage of individual components during their preparation (Fig. S4 and S5, ESI†). Also, we carried out PL experiments at 364 nm excitation varying the slit width of excitation and emission windows (Fig. S6, ESI†), and observed characteristic emission peaks of Eu^{3+}. However, the intensity of peaks decreases with decrease of slit width. The absorption peak at around 364 nm is due to Eu^{3+} (Fig. S7, ESI†), but its intensity is much less than that of 395 nm.

The fluorescence microscopy image (Fig. S8, ESI†) clearly shows good luminescent imaging capability of MLHN mounted on glass slide. Thus, we have investigated the cellular imaging capability of these MLHN using CLSM (Fig. 8) in A549 cells during culture conditions. A significant uptake/spatial distribution of hybrid nanostructures were clearly observed from the red luminescence image arising from MLHN emission. The blue and green

Table 1. The wavelengths corresponding to magnetic and electric dipole transitions of Eu^{3+} in AFLN and MLHN along with their asymmetric ratio (A_{21}).

Samples at different excitation wavelengths		Magnetic dipole transition ($^5D_0 \rightarrow {}^7F_1$)	Electric dipole transition		Asymmetric ratio (A_{21})
			$^5D_0 \rightarrow {}^7F_2$	$^5D_0 \rightarrow {}^7F_4$	
AFLN	260 nm	592 nm	616 nm	695 nm	0.96
	395 nm	592 nm	616 nm	695 nm	0.93
MLHN	260 nm	587 nm	612 nm	692 nm	0.91
	395 nm	589 nm	612 nm	692 nm	0.89

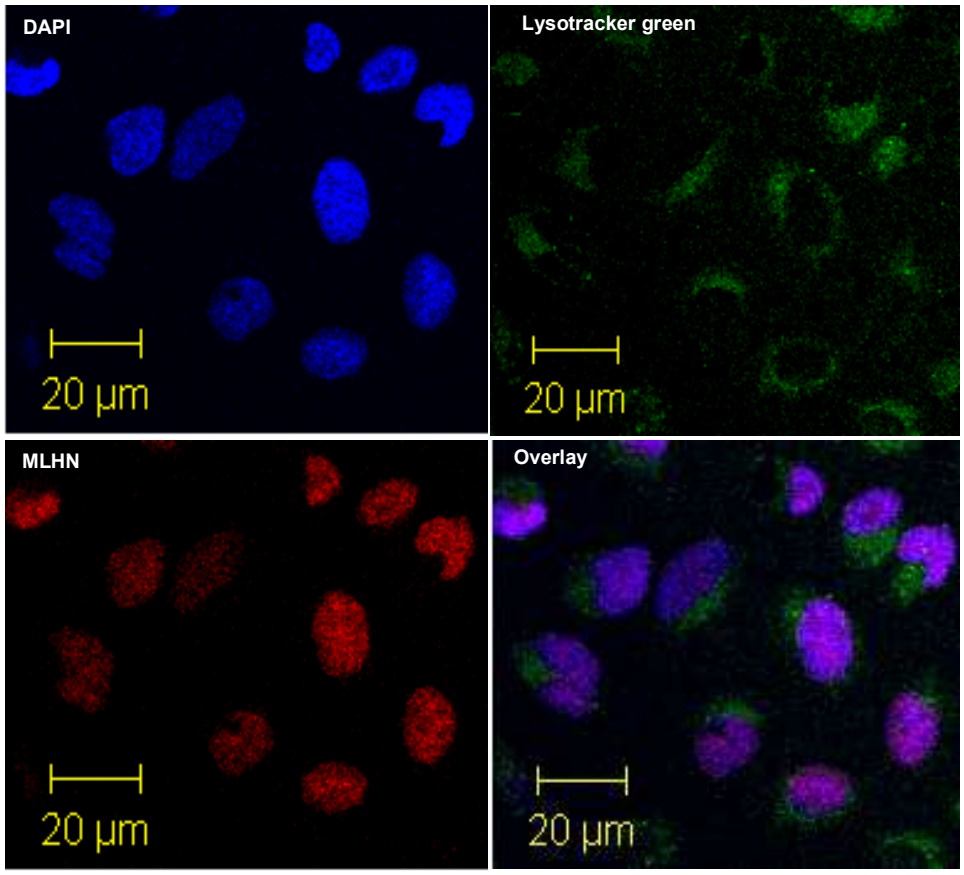

Fig. 8. CLSM images of A549 cells after treated with 1 mg of MLHN in culture condition and mounted in presence of DAPI and lysotracker green.

fluorescence images show emission from nucleus and lysosome stained with DAPI and lysotracker, respectively. The overlay image of MLHN, DAPI and lysotracker fluorescence (as seen by the magenta colour) clearly indicates that MLHN are co-localized in nucleus. This result clearly suggested that hybrid nanostructures are significantly internalized in the tumor cells and thus, they can be used as a potential marker/ tool for cellular imaging. However, further studies are required to understand the mechanism of cellular internalization.

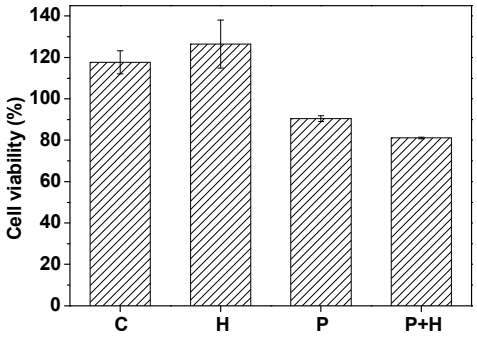

Fig. 9. Viability of A549 cells upon exposure of AMF (0.335 kOe) for 10 min in presence of MLHN with respective controls.

We have also studied their hyperthermic tumor cell killing efficiency in A549 cells in presence and absence of AMF (Fig. 9). It has been observed that the control cells (C) and cells treated with AMF only (H) did not show any decrease in the percentage cell viability. However, the cells treated with MLHN showed a slight decrease in viability as compared to the control. It is worth mentioning that MLHN under AMF (P+H) showed further decrease of about 10 % in cell viability for 2 mg/ml of MLHN. The cell killing efficiency can be enhanced by increasing the weight percentage of magnetic particles in the hybrid nanostructure. Specifically, this study demonstrates the potential of these hybrid nanostructures for hyperthermia treatment of cancer cells.

Furthermore, we have investigated the interaction of MLHN with BSA protein in physiological medium (PBS-7.3). The MLHN-BSA (Table S1) does not show any significant change in zeta-potential of MLHN in physiological medium even after incubation for 2h. These results suggest that MLHN has negligible interaction with BSA protein. However, further studies are required to confirm the protein resistance properties of MLHN using serum or plasma samples. Specifically, the present study demonstrates successful synthesis of Fe_3O_4 decorated YPO_4: Eu hybrid nanostructure, which may have potential application in cellular imaging and hyperthermia therapy.

Conclusions

Aqueous stabilized, bifunctional Fe_3O_4 decorated YPO_4: Eu hybrid nanostructure was successfully synthesized by covalent conjugation of carboxyl PEGylated Fe_3O_4 and aminosilane functionalized YPO_4: Eu. Detailed structural characterizations confirmed the functionalization of individual counterparts as well as their successful conjugation through amide linkage. XRD and TEM analysis revealed the formation of highly crystalline hybrid nanostructures. It has been observed that 10 nm Fe_3O_4 nanoparticles are randomly distributed on the surface of 100-150 nm rice grain shaped YPO_4: Eu nanostructures. The hybrid nanostructures show superparamagnetic behaviour at 300 K and ferromagnetic behaviour at 5 K with a blocking temperature of 220 K. Emission spectra of these hybrid nanostructures exhibit typical emission peak of Eu^{3+} corresponding to the magnetic and electric dipole transitions. Thus, these hybrid nanostructures provide excellent platform to integrate both magnetic and luminescent properties into single entity. These MLHN also have better aqueous colloidal stability and excellent localized heating efficacy under external AC magnetic field, which indicates their potential application in hyperthermia treatment of cancer. Further, the fluorescent imaging capability of hybrid nanostructures can be used for cellular imaging. In addition, the high density of functionalized exteriors (free carboxyl and amine groups) on the surface of hybrid nanostructures can be accessed for conjugation of drugs/ biomolecules for other biomedical applications, such as targeted drug delivery, magnetic biolabeling and efficient bioseparation.

Acknowledgements

Authors thank Dr. B. N. Jagatap, Director, Chemistry Group and Dr. V. K. Jain, Head, Chemistry Division, BARC for the encouragement and support. The authors also thank Mr. Manjoor Ali and Ms. Vasumathy Pillai for confocal laser scanning microscopy studies.

Notes and references

1. C. D. Hu, A. Hu, L. Zhang and W. Lin, *J. Am. Chem. Soc.*, 2005, **127**, 12486.
2. L. Quinti, R. Weissleder and C. H. Tung, *Nano Lett.*, 2006, **6**, 488.
3. R. Weissleder, *Science*, 2006, **312**, 1168.
4. S. A. Corr, Y. P. Rakovich and Y. K. Gun'ko, *Nanoscale Res. Lett.*, 2008, **3**, 87.
5. X. L. Liu, H. M. Fan, J. B. Yi, Y. Yang, E. S. G. Choo, J. M. Xue, D. D. Fan and J. Ding, *J. Mater. Chem.*, 2012, **22**, 8235.
6. K. C. Barick, S. Singh, N. V. Jadhav, D. Bahadur, B. N. Pandey and P. A. Hassan, *Adv. Funct. Mater.*, **22** (2012) 4975.
7. V. M. Khot, A. B. Salunkhe, N. D. Thorat, R. S. Ningthoujam and S. H. Pawar, *Dalton Trans*., 2013, **42**,1249.
8. K. C. Barick, S. Singh, D. Bahadur, M. A. Lawande, D. P. Patkar and P. A. Hassan, *J. Colloid Interf. Sci.*, 2014, **418**, 120.
9. H. Gu, K. Xu, C. Xu and B. Xu, *Chem. Commun.*, (2006) 941.
10. S. Rana, N. V. Jadhav, K. C. Barick, B. N. Pandey and P. A. Hassan, *Dalton Trans.*, 2014, **43**, 12263.
11. N. K. Prasad, K. Rathinasamy, D. Panda and D. Bahadur, *J. Mater. Chem.*, 2007, **17**, 5042.
12. J. Van der Zee, *Ann. Oncol.*, 2002, **13**, 1173.
13. M. Mahmoudi, V. Serpooshan and S. Laurent, *Nanoscale*, 2011, **3**, 3007.
14. P. Sharrna, S. Brown, G. Walter, S. Santra and B. Moudgil, *Adv. Colloid Interface Sci.*, 2006, **123**, 471.
15. Z. Y. Ma, D. Dosev, M. Nichkova, S. J. Gee, B. D. Hammock and I. M. Kennedy, *J. Mater. Chem.*, 2009, **19**, 4695.
16. R. Hardman, *Environ. Health Perspect.*, 2006, **114**, 165
17. A. M. Derfus, W. C. W. Chan and S. N. Bhatia, *Nano Lett.*, 2004, **4**, 11
18. W. Di, J. Li, N. Shirahatam, Y. Sakka, M. Willingere and N. Pinna, *Nanoscale,* 2011, **3**, 1263.
19. W. Wang, M. Zou and K. Chen, *Chem. Commun.*, 2010, **46**, 5102.
20. A. I. Prasad, A. K. Parchur, R. R. Juluri, N. Jadhav, B. N. Pandey, R. S. Ningthoujam and R. K. Vatsa, *Dalton Trans.*, 2013, **42**, 4885.
21. C. Mi, J. Zhang, H. Gao, X. Wu, M. Wang, Y. Wu, Y. Di, Z. Xu, C. Mao and S. Xu, *Nanoscale*, 2008, **2**, 1141.
22. S. Rana, N. V. Jadhav, K. C. Barick, B. N. Pandey and P. A. Hassan, *Dalton Trans.*, 2014, **43**, 12263.
23. S. Nigam, K. C. Barick and D. Bahadur, *J. Magn. Magn. Mater.,* 2011, **323**, 237.
24. E. Occhipinti, P. Verderio, A. Natalello, E. Galbiati, M. Colombo, S. Mazzucchelli, A. Salvad, P. Tortora, S. M. Doglia and D. Prosperi, *Nanoscale*, 2011, **3**, 387.
25. F. Hu, K. W. MacRenaris, E. A. Waters, E. A. Schultz-Sikma, A. L. Eckermann and T. J. Meade, *Chem. Commun.*, 2010, **46**, 73.
26. A. K. Parchur, A. I. Prasad, S. B. Rai, R. Tewari, R. K. Sahu, G. S. Okram, R. A Singh and R. S. Ningthoujam, *AIP Advances*, 2012, **2**, 032119.
27. L. D. White and C. P. Tripp, *J. Colloid. Interf. Sci.*, 2000, **232**, 400.
28. B. Pan, D. Cui, F. Gao and R. He, *Nanotechnology*, 2006, **17**, 2483.
29. J. E. Wong, A. K. Gaharwar, D. Müller-Schulte, D. Bahadur and W. Richtering, *J. Nanosci. Nanotechnol*., 2008, **8**, 4033.
30. M. Mikhaylova, D.Y. Kim, N. Bobrysheva, M. Osmolowsky, V. Semenov, T. Tsakalakos and M. Muhammed, *Langmuir*, 2004, **20**, 2472.
31. P. Sharma, S. Rana, K. C. Barick, C. Kumar, H. G. Salunke and P. A. Hassan *New J. Chem.,* 2014, **38**, 5500.
32. A. Tomitaka, T. Koshi, S. Hatsugai, T. Yamada and Y. Takemura, *J. Magn. Magn. Mater.,* 2011, **323**, 1398.
33. B. Samanta, H. Yan, N. O. Fischer, J. Shi, D. J. Jerry and V. M. Rotello, *J. Mater. Chem.*, 2008, **18**, 1204.
34. N. K. Sahu, R. S. Ningthoujam and D. Bahadur, *J. Appl. Phys.*, 2012, **112**, 014306.
35. Y. S. Chang, H. J. Lin, Y. L. Chai and Y. C. Li, *J. Alloys Compd.*, 2008, **460**, 421.
36. M. N. Luwang, R. S. Ningthoujam, Jagannath, S. K. Srivastava and R. K. Vatsa, *J. Am. Chem. Soc.*, 2010, **132**, 2759.
37. A. K. Parchur, R. S. Ningthoujam, S. B. Rai, G. S. Okram, R. A. Singh, M. Tyagi, S. C. Gadkari and R. K. Vatsa, *Dalton Trans.*, 2011, **40**, 7595.
38. Q. Luo, S. Shen, G. Lu, X. Xiao, D. Mao and Y. Wang, *J. Mater. Chem.,* 2009, **19**, 8079.

Covalent Bridging of Surface Functionalized Fe_3O_4 and YPO_4: Eu Nanostructures for Simultaneous Imaging and Therapy

K. C. Barick[a,*], Anusha Sharma[a], Neena G. Shetake[b], R. S. Ningthoujam[a], R. K. Vatsa[a], P. D. Babu[c], B. N. Pandey[b], P. A. Hassan[a,*]

[a]*Chemistry Division, Bhabha Atomic Research Centre, Mumbai – 400085, India*

[b]*Radiation Biology and Health Sciences Division, Bhabha Atomic Research Centre, Mumbai – 400085, India*

[c]*UGC-DAE Consortium for Scientific Research, Mumbai – 400085, India*

[*]Corresponding authors: E-mail: kcbarick@barc.gov.in (K. C. Barick), hassan@barc.gov.in (P. A. Hassan); Fax: + 91 22 2550 5151; Tel: + 91 22 2559 0284

Graphical Abstract

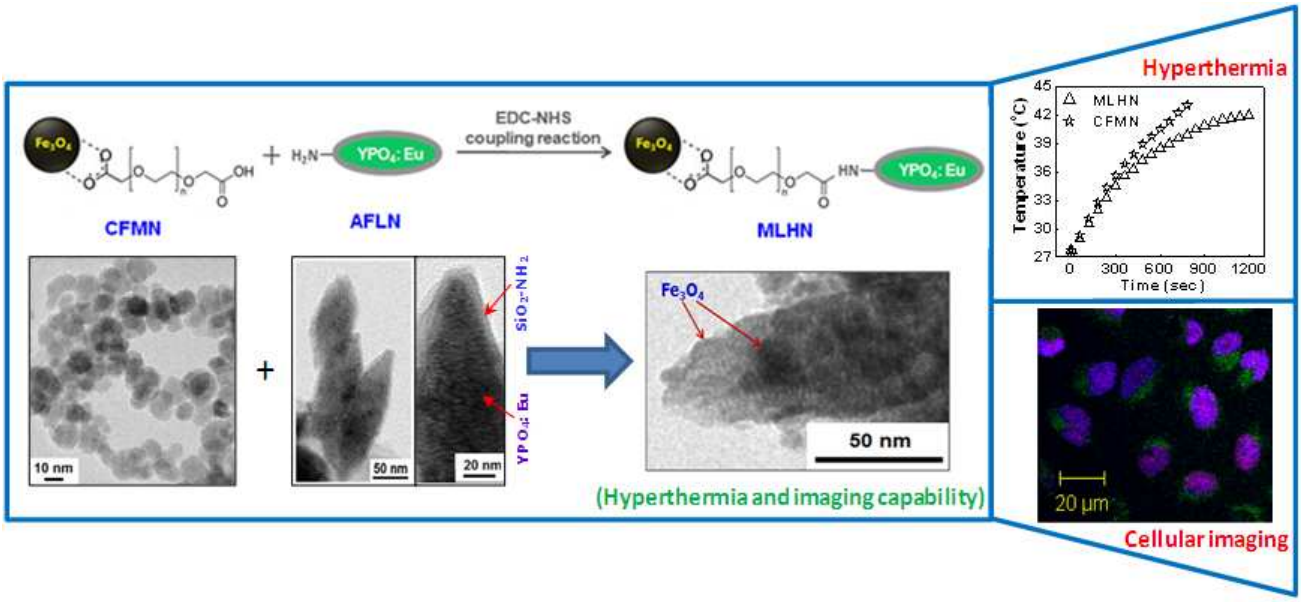

Development of Fe_3O_4 decorated YPO_4: Eu magnetic luminescent hybrid nanostructures (MLHN) for hyperthermia therapy and cellular imaging.